Supporting Information for:

Effect of Ionic Size on Solvate Stability of Glyme-Based Solvate Ionic Liquids

Toshihiko Mandai,[†,‖] Kazuki Yoshida,[†] *Seiji Tsuzuki*,[‡] Risa Nozawa,[†] Hyuma Masu,[§] *Kazuhide Ueno*,[†] *Kaoru Dokko*,[†,¶] *and Masayoshi Watanabe*[†,*]

[†]Department of Chemistry and Biotechnology, Yokohama National University, 79-5 Tokiwadai, Hodogaya-ku, Yokohama 240-8501, Japan

[‡]National Institute of Advanced Industrial Science and Technology (AIST), Tsukuba Central 2, Tsukuba, Ibaraki 305-8568, Japan

[§]Center for Analytical Instrumentation, Chiba University, 1-33 Yayoi-cho, Inage-ku, Chiba 263-8522, Japan

[¶]Unit of Elements Strategy Initiative for Catalysts & Batteries (ESICB), Kyoto University, Kyoto 615-8510, Japan

[‖]Present address: Department of Applied Physics, Chalmers University of Technology, Göteborg SE-412 96, Sweden

The complete analytical data are summarized here. Crystallographic data and thermal ellipsoid models for $[Li(G5)_1][TFSA]$, $[K(G5)_1][TFSA]$, $[Li(12C4)_1][TFSA]$, $[K(18C6)_1][TFSA]$, $[K(G4)_2]PF_6$, $[K(G5)_1]PF_6$, and $[K(G6)_1]PF_6$ are shown in **Table S1** and **Figures S1–S7**, respectively. Selected K–O_{glyme} distances are listed in **Table S2**. The HOMO energy levels of the deformed glymes are summarized in **Table S3**. Raman spectra of the crown ether–based complexes (**Figure S8**) and $[Li(G2)_2][TFSA]$ (**Figure S9**), the relative intensity of the selected bands (**Figure S10**), and optimized structures of the parent M[TFSA] salts (**Figure S11**) are also included. The complete author list for ref. 50 in the manuscript is given.

Table S1. Crystallographic data for $[Li(G5)_1][TFSA]$, $[K(G5)_1][TFSA]$, $[Li(12C4)_1][TFSA]$, $[K(18C6)_1][TFSA]$, $[K(G5)_1]PF_6$, and $[K(G6)_1]PF_6$.

	$[Li(G5)_1][TFSA]$	$[K(G5)_1][TFSA]$	$[Li(12C4)_1][TFSA]$	$[K(18C6)_1][TFSA]$	$[K(G5)_1]PF_6$	$[K(G6)_1]PF_6$
Chemical formula	$C_{14}H_{26}F_6LiNO_{10}S_2$	$C_{14}H_{26}F_6KNO_{10}S_2$	$C_{10}H_{16}F_6LiNO_8S_2$	$C_{14}H_{24}F_6KNO_{10}S_2$	$C_{12}H_{26}F_6KO_6P$	$C_{14}H_{30}F_6KO_7P$
Formula weight	553.42	585.57	463.29	525.41	450.40	494.45
Crystal system	Triclinic	Triclinic	Triclinic	Triclinic	Orthorhombic	Monoclinic
Space group	$P\bar{1}$	$P\bar{1}$	$P\bar{1}$	$P\bar{1}$	*Pbca*	$P2_1/c$
a / Å	9.2411(5)	9.430(2)	8.838(3)	8.7544(11)	15.404(3)	17.084(4)
b / Å	9.6767(5)	16.507(3)	9.535(3)	8.9026(13)	15.758(3)	13.0183(3)
c / Å	13.9904(7)	18.079(3)	11.379(4)	9.125 (2)	16.510(3)	20.904(5)
α / °	95.234(3)	66.416(6)	81.162(9)	113.587(5)	90	90
β / °	97.155(3)	78.330(8)	78.012(9)	95.750(6)	90	105.027(3)
γ / °	95.662(3)	81.019(8)	79.457(9)	106.5676(11)	90	90
V / Å^3	1228.46(11)	2517.1(8)	915.5(5)	605.8 (2)	4007.6(11)	4547(2)
Z	2	4	2	1	8	8
D_{calc} / g cm^{-3}	1.496	1.545	1.680	1.599	1.493	1.444
μ / mm^{-1}	0.2836	0.4679	0.3885	0.4858	0.4229	0.3829
Temp. / ºC	−50	−100	−100	−100	−100	−50
Reflections collected	8857	19189	7425	4532	29013	38408
Independent reflection, R_{int}	4307, 0.0285	11214, 0.0349	4562, 0.0230	2680, 0.0263	4580, 0.0363	12504, 0.0845
R_1 [$I > 2\sigma(I)$]	0.0631	0.0695	0.0424	0.0613	0.0656	0.0903
wR_2 (all data)	0.1733	0.2051	0.1248	0.2300	0.1761	0.2446
GooF	1.043	1.092	1.058	0.959	1.128	1.052

Table S2. Distances between the K^+ cation and oxygen atoms of the coordinating glymes in $[K(G4)_2]PF_6$, $[K(G5)_1]PF_6$, and $[K(G6)_1]PF_6$ solvates. Atomic numbering corresponds to the numbering in the corresponding crystallographic structure.

Distances / Å	$[K(G4)_2]PF_6$	$[K(G5)_1]PF_6$	$[K(G6)_1]PF_6$
K1−O1	2.877(5)	2.8201(19)	2.819(4)
K1−O2	3.013(5)	2.9100(19)	2.802(4)
K1−O3	3.069(4)	2.8648(18)	2.811(4)
K1−O4	2.981(5)	2.8322(17)	2.849(4)
K1−O5(13)	2.936(4)	2.8807(18)	2.833(3)
K1−O6		2.9069(19)	2.875(3)
K1−O7			2.962(4)

Table S3. HOMO energy levels of deformed glymes calculated via HF/6-311G** level *ab initio* molecular orbital calculations. The words in parentheses indicate the conformational form of the glymes and coordinated cationic species.

Samples	Atomic unit	eV	ΔeV_{trans}[a]
G3 (all *trans*)	−0.42093	−11.45	0
G3 (*deformed*, Li)[b]	−0.39277	−10.69	0.77
G3 (*deformed*, Li)[c]	−0.39763	−10.82	0.63
G4 (all *trans*)	−0.42116	−11.46	0
G4 (*deformed*, Li)[b]	−0.38678	−10.52	0.94
G4 (*deformed*, Li)[c]	−0.38818	−10.56	0.90
G4 (*deformed*, Na)	−0.39775	−10.82	0.64
G5 (all *trans*)	−0.42133	−11.46	0
G5 (*deformed*, Na)	−0.39437	−10.73	0.73
G5 (*deformed*, K)	−0.39987	−10.88	0.58

[a]ΔeV is the change in the HOMO level of the glymes associated with deformation upon complexation from that of the isolated *all trans* glymes.

[b, c]The optimized structures are obtained from refs. 18 and 51 in the manuscript, respectively.

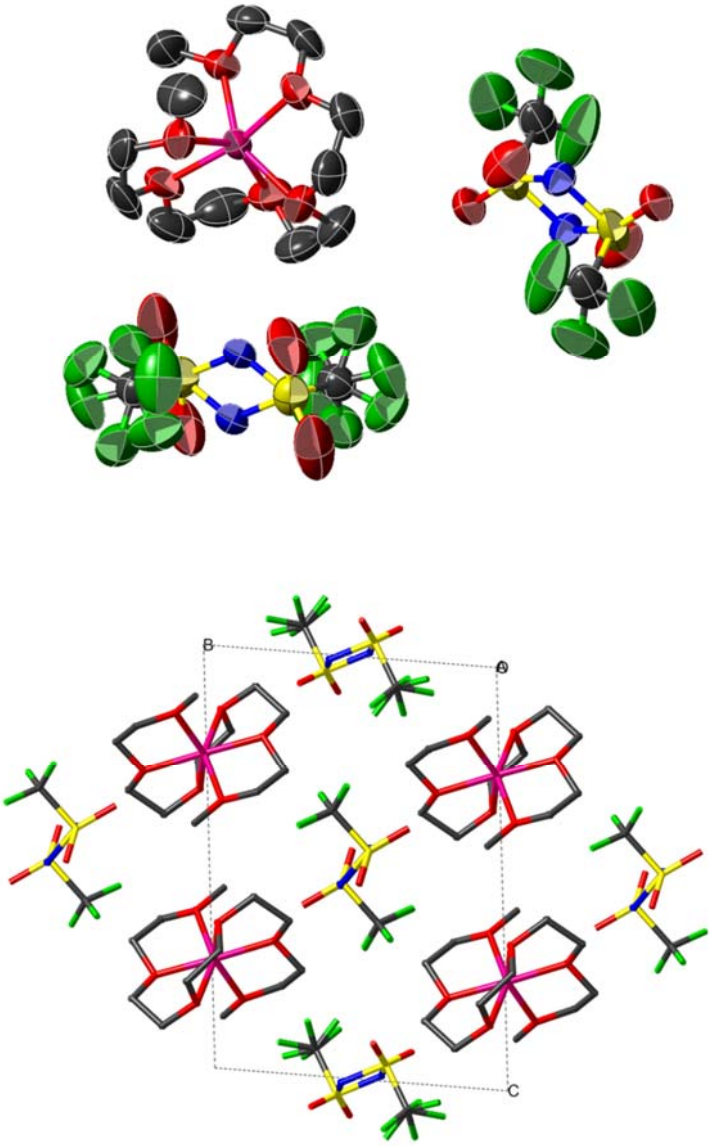

Figure S1. Thermal ellipsoid model (upper) and packing structure along the *a*-axis (lower) of $[Li(G5)_1][TFSA]$. The ellipsoids of non-hydrogen atoms are drawn at the 50% probability level. The expanded structures are shown here. H atoms and labels are omitted for clarity. Pink, Li; blue, N; yellow, S; red, O; green, F; gray, C; light gray, H. CCDC number: 1016396.

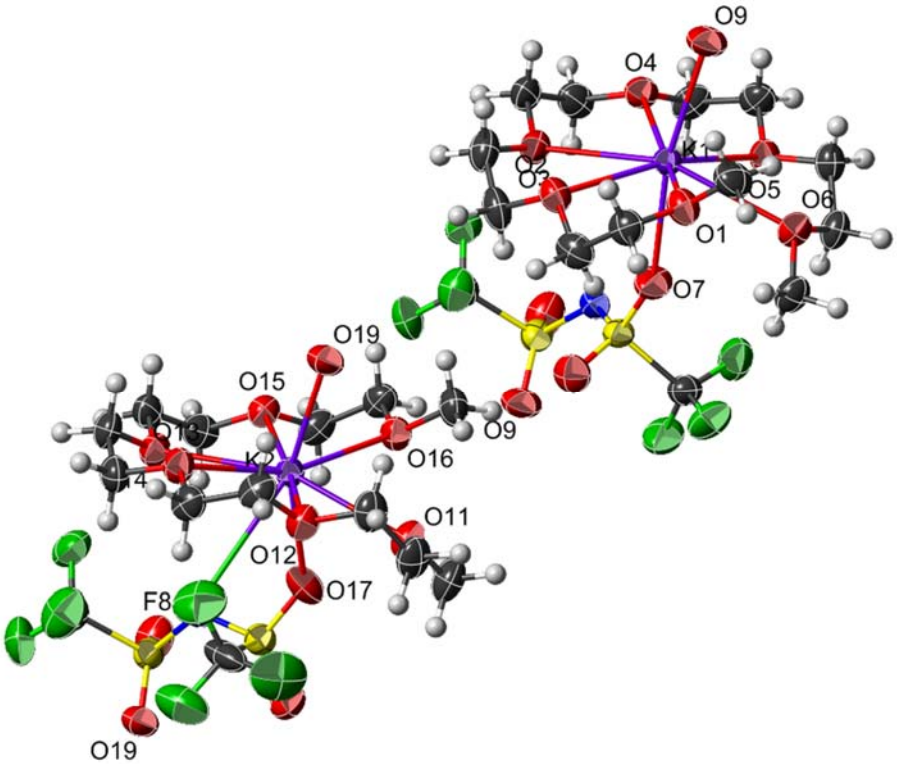

Figure S2. Thermal ellipsoid model of [K(G5)$_1$][TFSA]. The ellipsoids of non-hydrogen atoms are drawn at the 50 % probability level while isotropic hydrogen atoms are represented by spheres of arbitrary size. The labels of uncoordinating atoms are omitted for clarity. There are two types of AGG solvates (one is octa-coordinated and the other is nona-coordinated) in this solvate. Purple, K; blue, N; yellow, S; red, O; green, F; gray, C; light gray, H. CCDC number: 1016397.

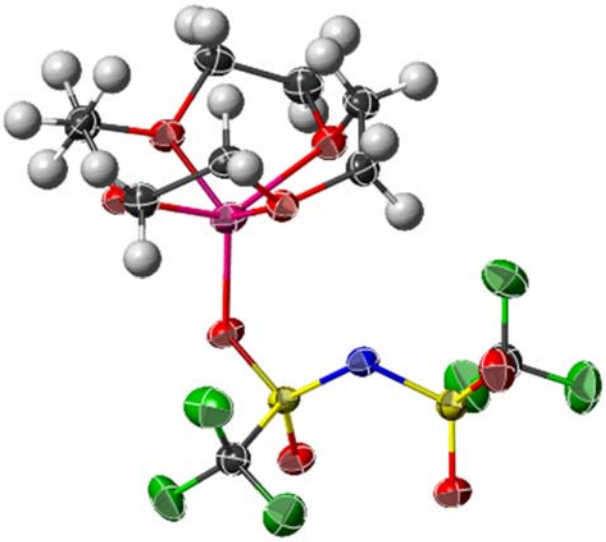

Figure S3. Thermal ellipsoid model of $[Li(12C4)_1][TFSA]$. The ellipsoids of non-hydrogen atoms are drawn at the 50% probability level while isotropic hydrogen atoms are represented by spheres of arbitrary sizes. The labels are omitted for clarity. Pink, Li; blue, N; yellow, S; red, O; green, F; gray, C; light gray, H. CCDC number: 1016398.

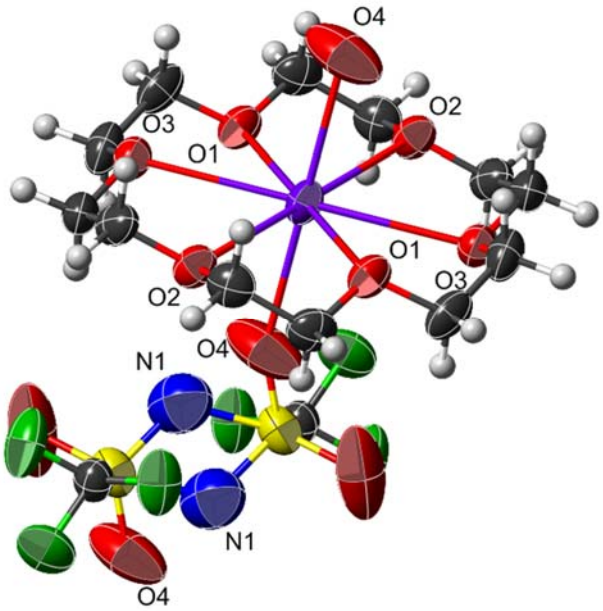

Figure S4. Thermal ellipsoid model of $[K(18C6)_1][TFSA]$. The ellipsoids of non-hydrogen atoms are drawn at the 50 % probability level while isotropic hydrogen atoms are represented by spheres of arbitrary size. The labels of uncoordinating atoms are omitted for clarity. The expanded structure is shown here. Purple, K; blue, N; yellow, S; red, O; green, F; gray, C; light gray, H. CCDC number: 1016399.

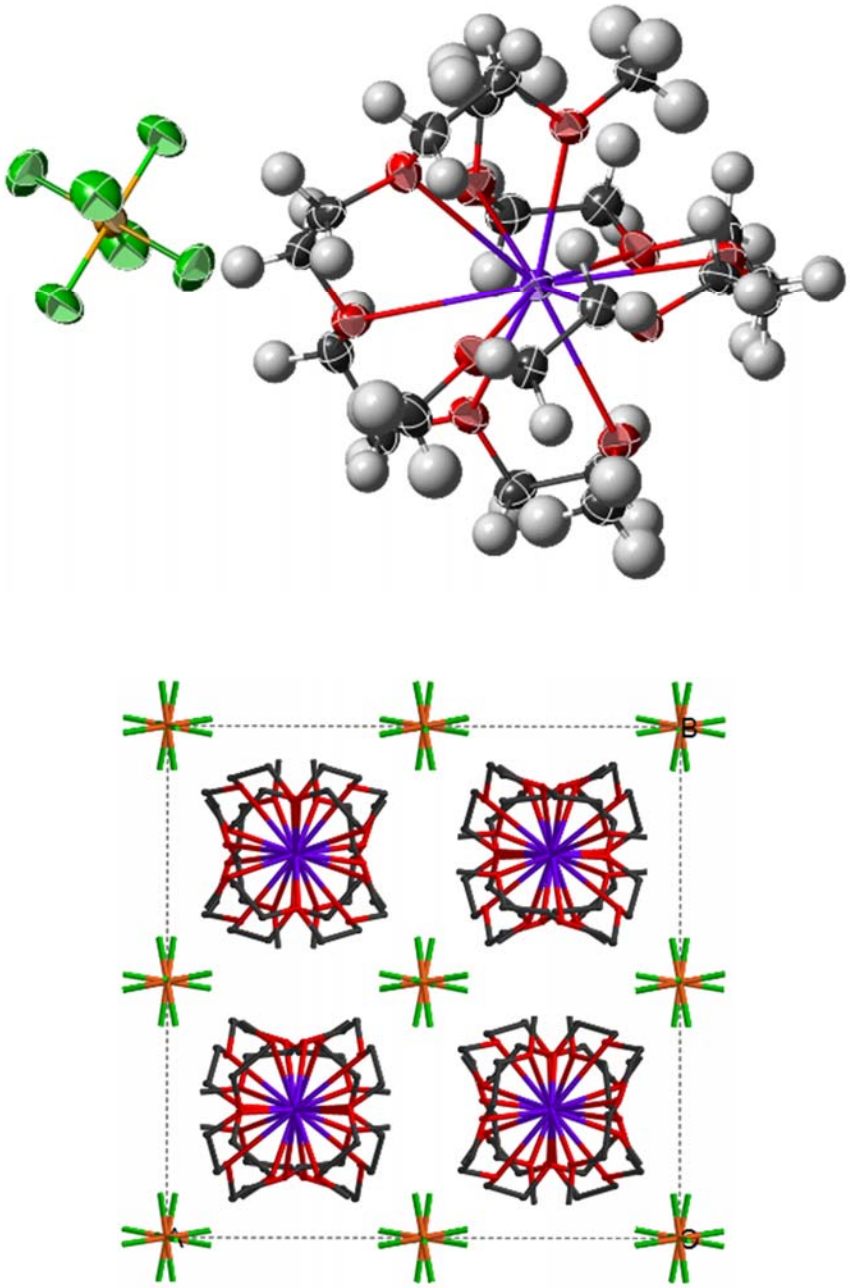

Figure S5. Thermal ellipsoid model (upper) and packing structure along the *c*-axis (lower) of $[K(G4)_2]PF_6$. The ellipsoids of non-hydrogen atoms are drawn at the 50% probability level while isotropic hydrogen atoms are represented by spheres of arbitrary sizes. The labels are omitted for clarity. Purple, K; orange, P; red, O; green, F; gray, C; light gray, H. Due to its high R_1 and $wR2$ values, this cif has not been deposited in the CCDC.

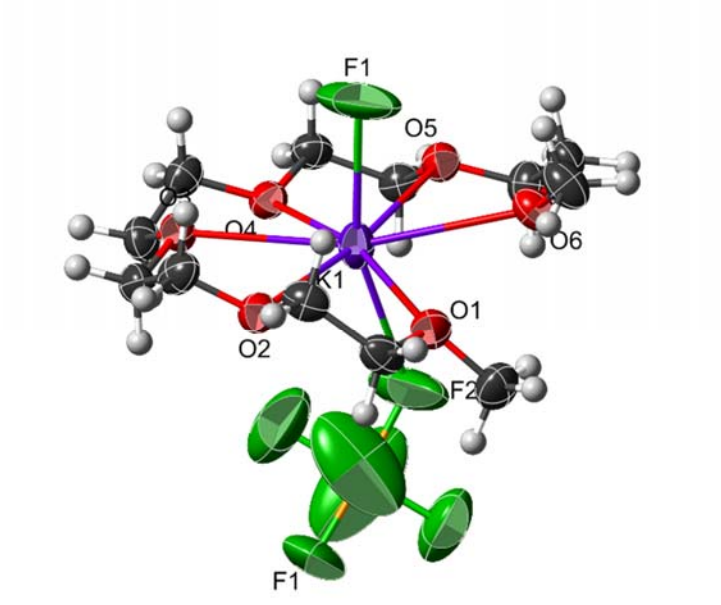

Figure S6. Thermal ellipsoid model of $[K(G5)_1]PF_6$. The ellipsoids of non-hydrogen atoms are drawn at the 50 % probability level while isotropic hydrogen atoms are represented by spheres of arbitrary size. The disordered atoms and labels of uncoordinating atoms are omitted for clarity. Purple, K; orange, P; red, O; green, F; gray, C; light gray, H. CCDC number: 1016400.

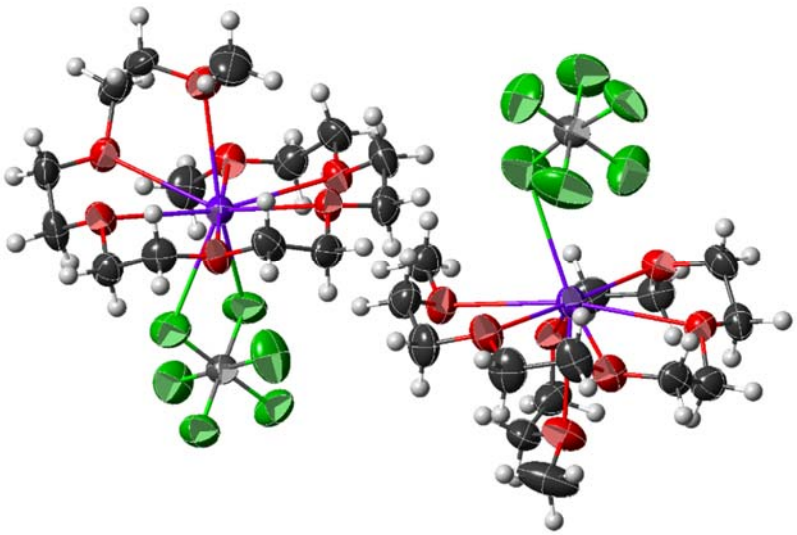

Figure S7. Thermal ellipsoid model of $[K(G6)_1]PF_6$. The ellipsoids of non-hydrogen atoms are drawn at the 50 % probability level while isotropic hydrogen atoms are represented by spheres of arbitrary size. Labels are omitted for clarity. Purple, K; orange, P; red, O; green, F; gray, C; light gray, H. CCDC number: 1016401.

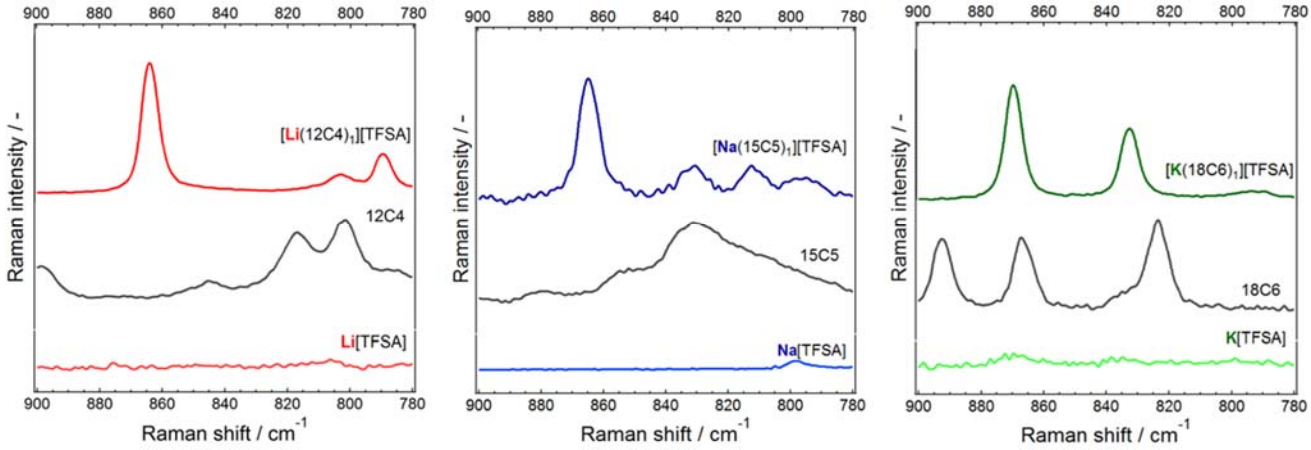

Figure S8. Raman spectra of crystalline $[Li(12C4)_1][TFSA]$, $[Na(15C5)_1][TFSA]$, and $[K(18C6)_1][TFSA]$ measured at ambient temperature. Spectra of each pure crown ether and parent salt are also included in each figure.

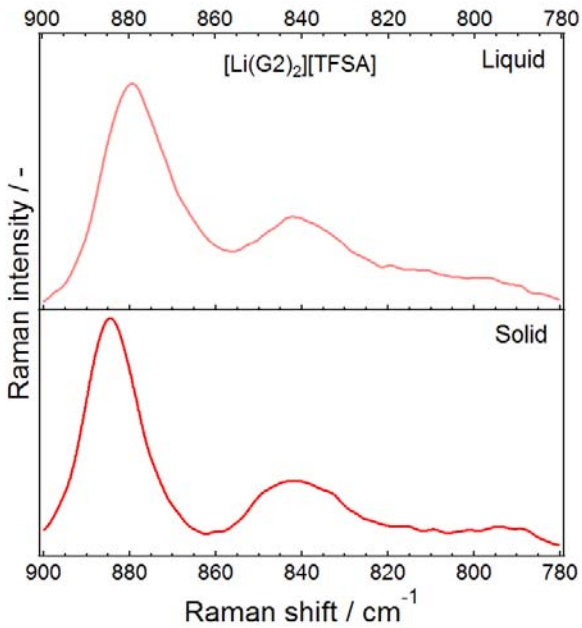

Figure S9. Raman spectra of $[Li(G2)_2][TFSA]$ in both crystalline (lower) and liquid (upper) states.

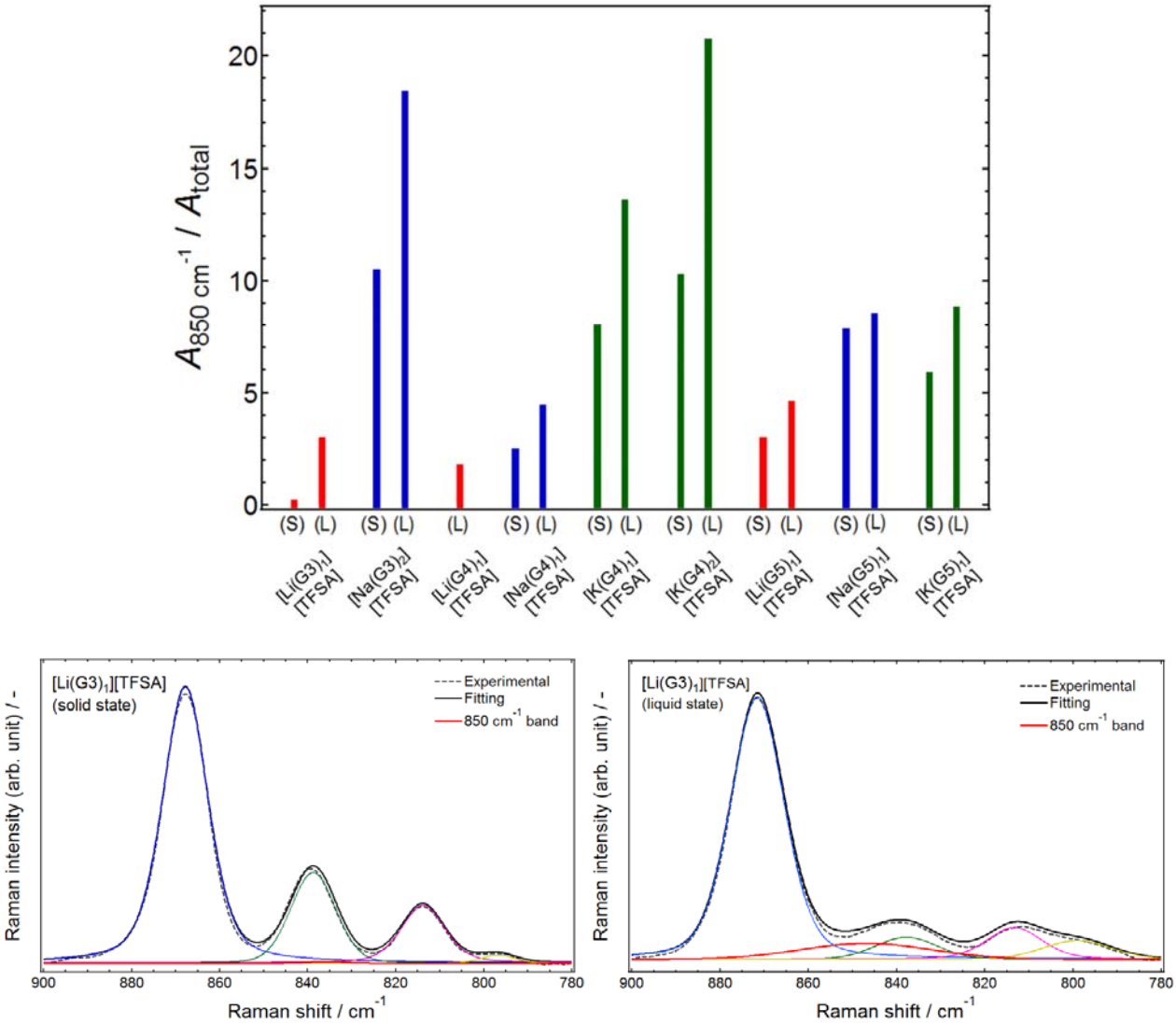

Figure S10. Variation of the relative intensity of the 850 cm^{-1} Raman band upon melting (upper). (S) and (L) indicate the solid and liquid states, respectively. The spectra were resolved into Gaussian-Lorentzian bands (examples are shown lower; $[Li(G3)_1][TFSA]$ in the solid (left) and liquid (right) states). $A_{850\ cm^{-1}}$ and A_{total} denote the peak areas assigned to free glyme that appeared at 850 cm^{-1} and all glymes observed at 900–780 cm^{-1}, respectively.

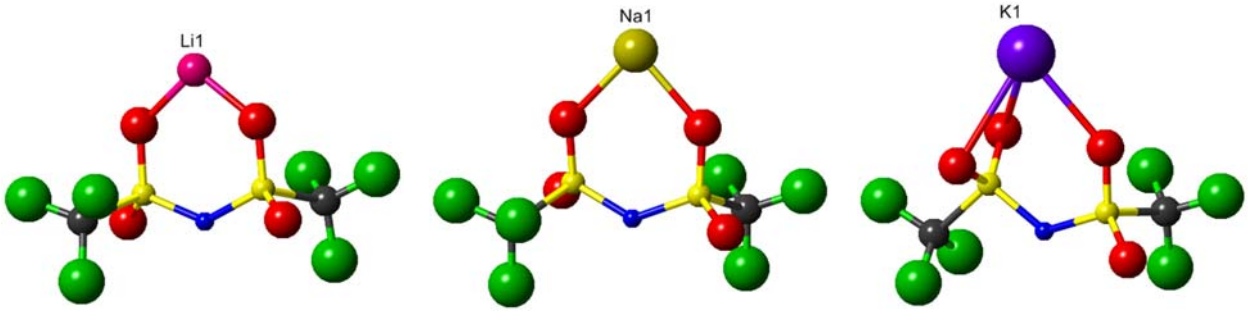

Figure S11. Optimized structures of Li[TFSA] (left), Na[TFSA] (center), and K[TFSA] (right) calculated via *ab initio* quantum calculation at the MP2/6-311G** level. Pink, Li; dark yellow, Na; purple, K; blue, N; yellow, S; red, O; green, F; gray, C. These figures are reproduced from ref. 66 in the manuscript.

Complete author list for the ref. 50 in the manuscript

50. Frisch, M. J.; Trucks, G. W.; Schlegel, H. B.; Scuseria, G. E.; Robb, M. A.; Cheeseman, J. R.; Montgomery, Jr., J. A.; Vreven, T,; Kudin, K. N.; Burant, J. C.; et al., Millam, J. M.; Iyengar, S. S.; Tomasi, J.; Barone, V.; Mennucci, B.; Cossi, M.; Scalmani, G.; Rega, N.; Petersson, G. A.; Nakatsuji, H.; Hada, M.; Ehara, M.; Toyota, K.; Fukuda, R.; Hasegawa, J.; Ishida, M.; Nakajima, T.; Honda, Y.; Kitao, O.; Nakai, H.; Klene, M.; Li, X.; Knox, J. E.; Hratchian, H. P.; Cross, J. B.; Bakken, V.; Adamo, C.; Jaramillo, J.; Gomperts, R.; Stratmann, R. E.; Yazyev, O.; Austin, A. J.; Cammi, R.; Pomelli, C.; Ochterski, J. W.; Ayala, P. Y.; Morokuma, K.; Voth, G. A.; Salvador, P.; Dannenberg, J. J.; Zakrzewski, V. G.; Dapprich, S.; Daniels, A. D.; Strain, M. C.; Farkas, O.; Malick, D. K.; Rabuck, A. D.; Raghavachari, K.; Foresman, J. B.; Ortiz, J. V.; Cui, Q.; Baboul, A. G.; Clifford, S.; Cioslowski, J.; Stefanov, B. B.; Liu, G.; Liashenko, A.; Piskorz, P.; Komaromi, I.; Martin, R. L.; Fox, D. J.; Keith, T.; Al-Laham, M. A.; Peng, C. Y.; Nanayakkara, A.; Challacombe, M.; Gill, P. M. W.; Johnson, B.; Chen, W.; Wong, M. W.; Gonzalez, C.; Pople, J. A. GAUSSIAN 03 (Revision E.01), Gaussian, Inc., Wallingford, CT, **2004**.